Atmospheric
Chemistry
and Physics
Discussions

Open Access

Dust-related ice nuclei profiles from polarization lidar: methodology and case studies

R. E. Mamouri[1] and A. Ansmann[2]

[1]Department of Civil Engineering and Geomatics, Cyprus University of Technology, Limassol, Cyprus
[2]Leibniz Institute for Tropospheric Research, Leipzig, Germany

Correspondence to: R. E. Mamouri (rodanthi.mamouri@cut.ac.cy)

Discussion Paper | Discussion Paper | Discussion Paper | Discussion Paper |

ACPD

14, 25747–25786, 2014

Dust-related ice nuclei profiling

R. E. Mamouri and A. Ansmann

Title Page

Abstract | Introduction

Conclusions | References

Tables | Figures

◄ | ►

◄ | ►

Back | Close

Full Screen / Esc

Printer-friendly Version

Interactive Discussion

Abstract

A lidar technique is presented that permits the estimation of ice nuclei concentrations of mineral dust from polarization lidar measurements. The method is applied to lidar observations of the spaceborne lidar CALIOP (Cloud Aerosol Lidar with Orthogonal Polarization) during two overpasses of the EARLINET (European Aerosol Research Lidar Network) lidar site at the Cyprus University of Technology (CUT), Limassol (34.7° N, 33° E), Cyprus. The good agreement between the CALIOP and CUT lidar observations regarding the retrieval of the aerosol particle concentration for particles larger than 280 nm in radius, APC_{280}, and the ice nuclei concentrations, INC, corroborates the potential of CALIOP to provide 3-D global dust-related INC data sets. The method makes use of the polarization lidar technique for the separation of dust and non-dust aerosol components. The profile of dust extinction coefficient is converted to APC_{280} and, in a second step, to INC by means of an APC–INC relationship from the literature. The observed close relationship between dust extinction at 500 nm and APC_{280} is the key to a successful INC retrieval. The correlation between dust extinction coefficient and APC_{280} is studied by means of AERONET sun/sky photometer at Morocco, Cape Verde, Barbados, and Cyprus, during situations dominated by desert dust outbreaks.

1 Introduction

The evolution of the ice phase in initially liquid-water clouds is still poorly understood and thus not well considered in climate models. Trustworthy predictions of the overall indirect aerosol effect on climate are impossible as long as the important branch of heterogeneous ice formation, the subsequent production of rain, and the associated removal of water from the atmosphere is not properly described in atmospheric circulation models. Aircraft-based field campaigns in cloudy environments are performed to improve the basic process understanding on heterogeneous ice formation at given meteorological and aerosol conditions. Laboratory studies and in situ aerosol charac-

terization provide important knowledge on the influence of a variety of natural and anthropogenic aerosol types on cloud glaciation. Lidar and radar-based remote sensing allows a detailed temporally and vertically resolved continuous monitoring of the evolution of the ice phase in cloud layers, and more generally of the life cycle of clouds. Active remote sensing seems to be very promising for a long-term monitoring of aerosol-cloud interactions (Shupe, 2007; Illingworth et al., 2007; Ansmann et al., 2009; Seifert et al., 2010; Martucci and O'Dowd, 2011; de Boer et al., 2011; Zhang et al., 2011; Kanitz et al., 2011; Wandinger et al., 2012; Bühl et al., 2013; Schmidt et al., 2014).

However, further efforts to improve the retrieved capabilities of active remote sensing are desirable. Regarding heterogeneous ice formation it is of interest to explore the potential of polarization lidar to deliver height profiles of ice nuclei concentrations (INC). Such an approach is presented here. The technique can be applied to any polarization lidar, i.e., also to CALIOP (Cloud Aerosol Lidar with Orthogonal Polarization) observations, so that global 3-D maps of INC can, in principle, be produced from the spaceborne lidar observations. CALIOP is part of the CALIPSO (Cloud-Aerosol Lidar and Infrared Pathfinder Satellite Observation) mission (Winker et al., 2009).

In this paper, we concentrate on desert-dust-related INC. Mineral dust (desert dust, soil dust) is the most important aerosol type with respect to heterogeneous ice formation (Richardson et al., 2007; Kamphus et al., 2010; Murray et al., 2012; Cziczo et al., 2013; DeMott et al., 2014). Besides deserts, Nisantzi et al. (2014) showed that also biomass burning around the globe may be an important source of soil dust. According to DeMott et al. (2014) all dust particles (of different origin) can be considered as single-type ice nucleating particles.

After a short introduction into the used instruments in Sect. 2, the INC retrieval method is explained in Sect. 3. A case study illustrates the procedure. In Sect. 4, the method is also applied to CALIOP observations performed during overpasses of the ground lidar station at Limassol, Cyprus. Summarizing and concluding remarks are given in Sect. 5.

2   Instrumentation

The lidar station of the Cyprus University of Technology (CUT) at Limassol (34.7° N, 33° E, 50 m a.s.l.) is located about 150 km south of Turkey and 250 km west of Syria and belongs to the European Aerosol Research Lidar Network (EARLINET). The lidar is described by Mamouri et al. (2013) and enables us to determine height profiles of the particle backscatter coefficient and particle linear depolarization ratio at 532 nm.

The ground-based lidar is collocated with a sun/sky photometer of the Aerosol Robotic Network (AERONET, CUT-TEPAK site, Limassol, Cyprus, http://aeronet.gsfc. nasa.gov) (Holben et al., 1998). The CUT AERONET photometer allows the retrieval of the aerosol optical thickness (AOT) at eight wavelengths from 339 to 1638 nm. Sky radiance observations at four wavelengths complete the AERONET observations. From these measurements the column-integrated particle size distribution is retrieved.

The spaceborne lidar CALIOP is described by Winker et al. (2009). This aerosol/cloud lidar measures polarization sensitive backscatter signals at 532 nm. CALIOP aerosol products include height profiles of the 532 nm particle backscatter coefficient, extinction coefficient, particle backscatter coefficient determined from the cross-polarized 532 nm signal channel, and the particle linear depolarization ratio. We use the CALIOP level 2 version 3 aerosol profile products. Besides the available profile of the particle depolarization ratio, we calculated this quantity in addition from the individual profiles of the cross-polarized and total 532 nm particle backscatter coefficients after smoothing of these individual profiles as suggested by Tesche et al. (2013).

3   Method

Table 1 provides an overview of all steps of the method applied to estimate dust-related INC values from polarization lidar measurements. In the first part (Sect. 3.1), we briefly describe how we obtain the dust-related backscatter coefficients for fine mode and coarse mode and the related dust extinction coefficients at 532 nm wavelength (steps

1-3 in Table 1). The second and essential part (Sect. 3.2) of the methodology deals with the link between the dust extinction coefficient for the 500-532 nm wavelength range and the aerosol particle number concentration, APC, for particles with radius $r > 280$ nm, denoted as APC_{280} (or $n_{d,280}$ in formulas). This fraction of large particles is the reservoir for favorable ice nuclei (IN) after DeMott et al. (2010) and allows us to directly estimate INC from APC_{280} for given ambient temperature conditions. This part of the retrieval is outlined in Sect. 3.3. We use APC_{280} instead of APC_{250} as originally suggested by DeMott et al. (2010) because the AERONET data base contains size distribution data sets for 22 size intervals from which APC_{280} (and not APC_{250}) can be directly computed. The full retrieval procedure is illustrated by means of a case study in Sect. 3.4.

3.1 Dust extinction from polarization lidar

The determination of the total particle backscatter coefficient, β_p, at 532 nm (step 1 in Table 1) from the elastic-backscatter lidar return signals is described by Mamouri et al. (2013). The separation of the backscatter components for non-dust aerosol particles, β_{nd}, fine-mode dust, β_{df}, and coarse-mode dust, β_{dc} (step 2 in Table 1), by means of the measured particle depolarization ratio is outlined in detail in Mamouri and Ansmann (2014). Fine-mode particles are defined as particles with radius < 500 nm. From the derived three components of the particle backscatter coefficient, we estimate the respective extinction coefficients for the non-dust aerosol component, σ_{nd}, fine dust, σ_{df}, and coarse dust, σ_{dc}, and finally we obtain the sum of the fine and coarse-mode dust extinction coefficients, $\sigma_d = \sigma_{df} + \sigma_{dc}$ (step 3 in Table 1). The total dust extinction coefficient σ_d is the basic information for the next steps, i.e., in the estimation of APC_{280} and INC. We ignore a potential spectral dependence of the dust extinction coefficient and assume no difference between the dust extinction coefficients derived from AERONET (500 nm) and CUT lidar observations (532 nm).

An example of the backscatter and extinction retrieval is shown in Fig. 1. Only the derived particle extinction coefficients for the different resolved aerosol types are pre-

Title Page

Abstract | Introduction

Conclusions | References

Tables | Figures

|◀ | ▶|

◀ | ▶

Back | Close

Full Screen / Esc

Printer-friendly Version

Interactive Discussion

sented. The (basic) solutions for the particle backscatter coefficients of the different aerosol components are shown in Fig. 15 of Mamouri and Ansmann (2014). The dust fraction is frequently also denoted as non-spherical particle fraction. The non-dust aerosol fraction, usually also denoted as the spherical particle fraction, includes
5   fine-mode anthropogenic haze and biomass burning smoke particles, which can be regarded as spherical particles with respect to their optical properties in the lidar signal analysis, as well as fine and coarse marine particles, which usually show a liquid shell according to numerous lidar observations around the world. Non-spherical non-mineral-dust aerosol components such as dried marine particles, pollen, biomass-
10   burning ash particles, and volcanic ash particles usually occur in rather low concentrations (except during pronounced volcanic eruptions and nearby fire events) and influence lidar observation in a negligible way. Backward trajectories are used to check a potential influence of these latter non-spherical aerosol particles on lidar observations and to avoid misinterpretation of dust measurements with lidar.
15   The observation in Fig. 1 was performed during a dust outbreak from deserts in the Middle East on 29 September 2011. Besides the separation of non-dust, fine dust, and coarse dust contributions to the total particle extinction coefficient by means of the recently introduced two-step method (right panel of Fig. 1), the so-called one-step method (center panel of Fig. 1) can also be applied to separate non-dust (spherical)
20   and dust (non-spherical) contributions to particle backscattering and extinction.

The one-step method (Tesche et al., 2009a; Mamouri and Ansmann, 2014) is well established. The dust and non-dust contributions to particle backscattering are separated here by means of the particle linear depolarization ratio (in one computational step) by assuming a depolarization ratio of $< 5\%$ for non-dust particles and $> 31\%$ for
25   desert dust particles (mostly coarse-mode particles). Depolarization ratios from 5-31 % indicate mixtures of dust and non-dust particles. In the case of the two-step algorithm, we separate non-dust particles (causing $< 5\%$ depolarization ratio), fine-mode dust (causing 16 % depolarization ratio), and coarse mode dust (causing 39 % depolariza-

tion ratio), in two successive steps as described in detail by Mamouri and Ansmann (2014).

We use the information from accompanying AERONET photometer observations to routinely check the reliability of the lidar retrieval products. The column-integrated fine-mode fractions (ratio of fine-mode AOT to total AOT), FMF, derived from the lidar data and from the AERONET observations are compared. In this comparison, we simply assume that non-dust particles (one-step method) or the sum of non-dust particles plus fine-mode dust (two-step method) cause the fine-mode AOT, whereas dust (one-step method) or coarse dust (two-step method) is the only significant contributor to the coarse-mode optical depth. As shown in Mamouri and Ansmann (2014), the column-integrated 500 nm FMF was 0.43 (AERONET observation), 0.18 (one-step lidar method), and 0.44 (two-step lidar method) for the case in Fig. 1. The two-step-method results are thus in better agreement with the photometer observations in this case. However, as will be shown in Sect. 3.2, the basis of the INC retrieval is the total (fine+coarse) dust extinction coefficient, which is almost equal for the solutions obtained with the one-step and two-step methods in the free troposphere. The further analysis shows that the total dust extinction coefficients can be obtained with an uncertainty of the order of 25-30 % (Tesche et al., 2009a; Mamouri and Ansmann, 2014).

3.2 Link between dust extinction and APC_{280}

In the next step of the retrieval (step 4 in Table 1), we investigate the relationship between the dust extinction coefficient at 500-532 nm (and 500 nm AOT) and the corresponding APC_{280}. A good relationship between the 500 nm AOT and the column-integrated APC_{280} is of key importance for the entire INC retrieval. We extensively analyzed AERONET sun/sky photometer observations at several sites with strong Saharan dust impact (Ouarzazate, Morocco, Praia, Cape Verde, and Barbados), and at Limassol, Cyprus. Limassol is frequently crossed by dense mineral dust layers originating from the Saharan desert as well as from the deserts in the Middle East. Details to these AERONET stations can be found on the AERONET web page

(http://aeronet.nasa.gov), in Mamouri and Ansmann (2014), and Toledano et al. (2009, 2011).

Figure 2 illustrates our approach to compute APC_{280}. Column-integrated particle volume size distributions measured during two dust outbreaks from the Middle East (1 November 2013 and 29 September 2011) and two from the Sahara (11 March and 2 June 2013) are presented. APC_{280} considers all radius intervals with interval mean radiis of 330 nm and larger. To obtain the particle number concentration for each interval, we divided the shown volume concentration by the volume of a single particle with a radius equal to the interval mean radius.

In Fig. 3, AERONET data of the correlation between the 500 nm AOT and APC_{280} from various field campaigns are shown. During the Saharan Mineral Dust Experiment 1 (SAMUM-1) (Toledano et al., 2009; Tesche et al., 2009b) in Morocco in the summer of 2006, many pure dust cases could be collected. A few, but heavy Saharan dust outbreaks were observed on 28 and 29 January 2008 at Praia, Cape Verde, during SAMUM-2 (Toledano et al., 2011; Tesche et al., 2011). Several dust-dominated cases measured at Barbados (AERONET-SALTRACE site) during the Saharan Aerosol Long-range Transport and Aerosol-cloud Interaction Experiment (SALTRACE) are included in Fig. 3. A good correlation between AOT and column APC_{280} is found for the dust observations in Morocco, Cape Verde, and Barbados.

Data from dust outbreaks towards Limassol, Cyprus, shown in Fig. 3, were measured in the years from 2011-2013. Because the contribution of anthropogenic aerosol pollution to the total AOT is generally large when the air masses are advected from the east, the correlation between AOT at 500 nm and column APC_{280} is comparably low over Cyprus. The correlation between the coarse-mode-related AOT and column APC_{280} is much better. The coarse-mode AOT is widely determined by light extinction by dust particles. From all the AERONET data in Fig. 3 we conclude that a clear and similar relationship between desert-dust APC_{280} and dust-related extinction coefficient exists.

Dust-related ice nuclei profiling

R. E. Mamouri and A. Ansmann

Title Page

Abstract	Introduction
Conclusions	References
Tables	Figures

|◀ ▶|

◀ ▶

Back Close

Full Screen / Esc

Printer-friendly Version

Interactive Discussion

Full Screen / Esc

Printer-friendly Version

Interactive Discussion

In the next step, we used the dust layer heights (DLH) which were simultaneously measured with lidar in Morocco, Cape Verde, and Barbados and formed the ratios of AOT to DLH and column APC_{280} to DLH to obtain the respective relationship between the dust layer mean APC_{280} and the respective dust layer mean extinction coefficient $\sigma_d(z)$. The result of the correlation of AOD/DLH with column-APC_{280}/DLH is shown in Fig. 4. The correlation coefficient is 0.91. Linear regression yield a clear relationship between the dust extinction coefficient and APC_{280} (step 5 in Table 1):

$$n_{d,280}(z) = c_{d,280} \cdot \left[\sigma_{df}(z) + \sigma_{dc}(z)\right] . \tag{1}$$

with $n_{d,280}$ in cm^{-3} at height z, the conversion factor $c_{d,280} = 0.673$ in Mm/cm^3, and the extinction coefficient σ in Mm^{-1}.

Based on the extended AERONET data set of dust observations in Fig. 3, we found that APC_{280} can be determined from the lidar-derived total dust extinction coefficient $\sigma_d(z)$ with an uncertainty of about 20 %. The overall uncertainty (standard deviation) in the APC_{280} values after Eq. (1) is thus about 30-40 %. Contributions to this error are the uncertainty of 25-30 % in the determination of dust extinction coefficient $\sigma_d(z)$ and 20 % in the conversion factor of $0.673\,cm^{-3}\,Mm$ in Eq. (1).

3.3 Estimation of INC from APC_{280}

In the final step 6 in Table 1, we estimate INC by means of the relationship (DeMott et al., 2010):

$$n_{IN}(z) = a\,[273.16 - T(z)]^b\, n_{d,280}(z)^{c[273.16 - T(z)]+d} \tag{2}$$

with $n_{d,280}$ in cm^{-3}, n_{IN} in L^{-1}, $a = 0.0000594$, $b = 3.33$, $c = 0.0265$, $d = 0.0033$, and temperature $T(z)$ in K (and < 273.16 K). Note that we use $n_{d,280}$ instead of $n_{d,250}$ as given in the original formula in DeMott et al. (2010). $n_{d,280}$ is roughly 10-15 % lower than $n_{d,250}$ for dust layers with strong coarse mode. Regarding uncertainties in the

INC estimation, DeMott et al. (2010) pointed out that Eq. (2) allows a prediction of INC within an uncertainty range of less than an order of magnitude, with the remaining variability apparently due to variations in aerosol chemical composition or other factors. By means of Eq. (2), 62 % of the observational data collected during nine field studies could be predicted within a factor of 2. These field studies were performed at a variety of locations around the globe over a 14 year period.

Equation (2) holds for the immersion freezing mode, the most important heterogeneous ice nucleation mode for temperatures down to at least −25 °C, and can be used for all aerosol types. There are other parameterizations from Niemand et al. (2012) and Tobo et al. (2013) which may be more applicable to mineral dust studies. These approaches produces up to an order of magnitude higher INC values than Eq. (2) (DeMott et al., 2014). However, the uncertainties in all parameterizations are large (within a factor of 10 or even larger). Thus the uncertainty in the INC estimation with Eq. (2) is presently assumed to be within an order of magnitude.

It should be emphasized that the main goal and importance of our work is the presentation and application of a retrieval scheme that allows us to obtain APC_{280} values from the desert-dust-related extinction coefficients which were derived before from the total particle extinction coefficients by means of the polarization lidar technique. Any of the available parameterizations to predict dust-related INC from APC_{250} or APC_{280} may be used in the next step to estimate INC profiles. We use Eq. (2) in the following presentation of ground-based and spaceborne lidar observations with the attempt to provide tropospheric INC profiles.

Concerning the uncertainties we can summarize that the retrieval of dust extinction coefficient is possible with a relative error of 25-30 %, the uncertainty in the conversion of the dust extinction coefficients into APC_{280} is about 20 %, and the uncertainty in the estimation of the INC profile is presently possible within an order of magnitude.

3.4 INC retrieval overview: CUT lidar case study

The concept to estimate INC from dust extinction coefficients via the determined AERONET-based relationship between 500 nm AOT and column-integrated APC_{280} was originally developed by Ansmann et al. (2008) and then further discussed by Seifert et al. (2011). Figure 5 provides an overview of the retrieval approach (steps 3–6 in Table 1) for the dust outbreak shown in Fig. 1. Dust extinction values observed during the Middle East desert dust outbreak towards Cyprus on 29 September 2011 range from 30-400 Mm^{-1}. An increase of dust extinction or APC_{280} by an order of magnitude corresponds to an increase in INC by a factor of 2, 5 and 10 at temperatures of -15, -25, and $-35\,°C$, respectively. A ten-degree decrease in temperature (equivalent to about 1000-1500 m height change in the free troposphere) leads to an increase in INC by a factor of 15-20 for a given APC_{280} according to Eq. (2). Thus, in cases of cloud convection, lifting of air parcels from below the cloud base towards the upper part of the cloud tower can lead to an enormous increase of the potential of a given dust load to initiate ice nucleation via immersion freezing.

The INC/APC_{280} ratio is about 1/200, 1/2000, and 1/40000 at -35, -25, and $-15\,°C$, respectively, for an APC_{280} around 100 cm^{-3}. Ansmann et al. (2008) assumed a much too large INC/APC ratio of 1/30 in their analysis of the impact of Saharan dust on cloud glaciation at temperatures from -10 to $-20\,°C$. This estimation was based on Saharan dust observations close to Florida (DeMott et al., 2003, 2006) however by ignoring any temperature dependence on the INC-APC relationship.

In Fig. 6, the relationship between INC, APC_{280}, and dust extinction coefficient shown in Fig. 5 is applied to the lidar dust profile measured on 29 September 2011. Height-independent temperature conditions are assumed to highlight the relative influence of a varying dust load with height on INC for a given temperature. However, again the comparably strong influence of temperature on INC is the dominant feature in Fig. 6, when comparing the three INC profiles for different temperatures.

As mentioned above and shown in Figs. 6 and 7, the one-step and the two-step methods lead almost to the same total dust extinction coefficient $\sigma_{d}(z)$ in the free troposphere above the marine boundary layer with top at about 400 m height. Both extinction profiles together show the possible solution range and thus the uncertainty in the dust extinction retrieval (Mamouri and Ansmann, 2014). Consequently, similar results in terms of INC are obtained with the one-step and two-step extinction method for the most interesting height range regarding heterogeneous ice formation.

Figure 7 shows INC profiles for the 29 September case for realistic vertical temperature distributions. Four midlatitude Standard Atmosphere temperature profiles defined by the surface temperature from −10 to 20 °C at 0 m height a.s.l. are considered. The actual air temperature at 2 m height above ground at Limassol on that day was close to 30 °C. For the corresponding temperature profile, INC is negligibly small at all heights throughout the entire troposphere. Therefore, we simulated these four temperature profiles for lower surface temperatures of 20, 10, 0, and −10 °C to obtain profiles with relevant INC levels. Again, the strong influence of ambient temperature on INC is visible. A significant increase of INC at all heights as shown in the figure may for example occur during the advection of air masses towards colder regions with less sun light so that radiative cooling and mixing with colder air masses may lead to a continuous and steady cooling of the dust-laden air mass. Note again the strong increase of INC with height in Fig. 7. This means that even traces of dust can have a strong impact on cloud glaciation when lifted in convective cloud towers (by several kilometers) or during long-range transport associated with large-scale lifting. The large dust particles may act as cloud condensation nuclei in the first step to form a liquid cloud environment, and may then become favorable immersion freezing nuclei after further lifting and cooling within the cloud tower.

4 Results

We applied our INC retrieval scheme to two CALIOP observations in the eastern Mediterranean close to Limassol, Cyprus. One of these overpasses took place during a strong Saharan dust outbreak on 1-2 June 2013. Traces of dust reached cirrus level (8-10 km height). During the second overpass, mineral dust was advected from the deserts in the Middle East on 1-2 November 2013. This second case can be regarded as representative for typical dust outbreaks with dust layers mainly in the lower free troposphere at heights between 1 and 5 km.

4.1 CALIOP and CUT lidar observations during a Saharan dust outbreak in June 2013

An overview of the dust and cloud observations of the spaceborne CALIOP lidar in the night of 1–2 June 2013 is shown in Fig. 8. The spaceborne lidar crossed eastern Ukraine (52-56° N), the Black Sea area (44-52° N), Turkey (36-42° N), the eastern Mediterranean Sea (30-36° N), Egypt (22-32° N), and Sudan ($< 22°$ N) within 12.5 min (corresponding to a distance of about 5000 km). The backward trajectory analysis in Fig. 9 indicates the southern parts of the Sahara as sources for the dust observed in the middle and upper troposphere over the eastern Mediterranean (above 2 km height).

Figure 10 compares the basic optical properties derived from the ground-based CUT lidar and the CALIOP observations close to Cyprus. A good agreement is visible when keeping different measurement and signal averaging periods (a few seconds in the case CALIOP, one hour in the case of the CUT lidar) and different locations of the two lidar instruments in mind. The nearest horizontal distance of the CALIOP laser foot print to Limassol was 45 km. Even small inhomogeneities in the horizontal distribution can easily explain the differences in the aerosol profiles observed with the two instruments.

For the INC retrieval, we smoothed the height profile of the particle backscatter coefficient measured with CALIOP with a vertical smoothing length of 600 m. To reduce the noise in the depolarization ratios, we smoothed the basic cross-polarized and total

particle backscatter coefficient profiles with 600 m smoothing length before the computation of the volume depolarization ratios and afterwards of the particle depolarization ratio. This procedure was recommended by Tesche et al. (2013). The left panel in Fig. 11 shows the basic CALIOP products (after 600 m smoothing). By applying the one-step and two-step methods described in Sect. 3.1 we obtain the dust particle extinction coefficient profiles shown in the central and right panels of Fig. 11. The solutions of the one-step and two-step methods are not in agreement at heights < 2km as is shown in Fig. 12. The uncertainty in the dust load occurs in a layer for which the backward trajectories suggest enhanced levels of anthropogenic aerosol pollution as well as of marine particles. The reasons for the resulting increased uncertainties are discussed by Mamouri and Ansmann (2014).

Figure 12 presents the results for this overpass case in terms of total (fine + coarse) dust extinction coefficient, APC_{280}, and INC for fixed height-independent temperatures. In this figure, we focus on the comparison of the results by applying the one-step and the two-step extinction retrieval methods. As mentioned before, the two techniques lead to significantly different total dust extinction profiles for heights < 2 km, but only small differences regarding the dust extinction profiles, APC_{280}, and INC at heights > 2 km, i.e., for the height range most relevant for heterogenous ice formation.

The importance of the 1–2 June 2013 case study lies in the fact that an unusually extended dust layer was detected. Dust was lifted to heights of 8-10 km height. Usually dust layers reach 5 km. As can be seen in Fig. 13, the potential of dust to initiate heterogeneous ice nucleation is increased by one to three orders of magnitude when the same amount of dust occurs at 9 km instead of 5 km height. As mentioned, such a strong increase of INC can occur when dust-laden air masses are lifted by several kilometers and respectively cooled by 10-20 K via updrafts in convective cumulus towers or via large-scale lifting (in front of warm fronts).

In Fig. 13, we compare the CALIOP retrieval results with the ones obtained with the ground-based CUT lidar. The two-step polarization lidar method is applied in the dust extinction retrieval. The agreement between the results is excellent. The comparably

high values of backscattering and extinction over Limassol seen by the CUT lidar below 1 km height are probably the result of enhanced levels of road dust and environmental dust over the city of Limassol. CALIOP was measuring over the open Mediterranean Sea east of Cyprus. Lidar overlap effects in the near range of the ground-based lidar

5 may have also contributed to the deviations between the different lidar observations at heights < 500 m.

4.2 CALIOP overpass during a dust outbreak from the Middle East in November 2013

Figure 14 provides an overview of the CALIOP measurements on 1 November 2013,

10 when a strong dust outbreak from deserts in the Middle East crossed Cyprus and the eastern Mediterranean (30-36° N). Figure 15 shows the comparison of basic CUT lidar and CALIPSO lidar products in terms of particle backscatter coefficient, extinction coefficient, and particle linear depolarization ratio. Lidar ratios of 40 sr were used here in the conversion of the backscatter into extinction values (Mamouri et al., 2013). Fig-

15 ure 16 presents HYSPLIT backward trajectories arriving at Limassol on 2 November 2013, 00:00 UTC. In contrast to the foregoing case study, dust was detected at heights below 4 km only.

The CALIOP data analysis was performed in the same way as in the case study discussed before in Sect. 4.1. The noisy CALIOP data profiles, averaged over 45 km

20 horizontal length, had to be smoothed with 600 m vertical window length. The obtained results are shown in Fig. 17.

As mentioned, the 1 November 2013 case is more representative for typical dust layering (with dust layer top heights below 5 km). At such conditions and surface temperatures of 20-30 °C, INC values are rather low throughout the dust plume. Ice formation

25 in altocumulus layers at the top of the dust layers (4-5 km above ground) is then almost impossible. This was already observed during the SAMUM-1 campaign and discussed by Ansmann et al. (2008). Only if cumulus convection at the top of the dust layers is strong enough so that the clouds can penetrate deeply into the free troposphere, dust

particles can act as effective ice nuclei (mainly triggering immersion freezing) because of the strongly decreasing ambient temperatures.

Figure 17 compares the CUT and CALIOP lidar findings for the dust outbreak from Middle East deserts. Again, the comparison between the CALIOP and CUT lidar products shows good agreement. Deviations can again be assigned to inhomogeneities in the horizontal dust distributions (over the 180 km distance of the CALIOP laser foot print from Limassol) and the rather different lidar signal averaging procedures (5 s, CALIOP, 60 min, CUT lidar).

5   Conclusions

For the first time, a lidar technique has been presented that allows us to estimate INC profiles from polarization lidar measurements. The approach paves the ground for INC vertical profiling as a support to ground-based and airborne in situ IN characterization and to conduct a global, vertically resolved mapping of dust-related INC by means of spaceborne lidar missions which may then allow an improved consideration of heterogeneous ice formation in atmospheric circulation models.

We applied the method to spaceborne CALIOP and ground-based CUT lidar measurements during overpasses of CALIOP of the eastern Mediterranean. Very different dust aerosol scenarios were observed with Saharan dust layers up to about 10 km height and Middle East desert dust plumes up to 4 km height. The case studies showed the dominant role of ambient air temperature in determining the INC characteristics of given dust plumes. However, strong dust outbreaks can significantly increase the potential of the atmosphere to initiate heterogeneous ice formation. On the other hand, even weak traces of dust may significantly impact cloud glaciation when air masses are lifted by several kilometers (convective lifting, large scale lifting in connection with frontal movements) and thus cooled down by 10-20 K.

The separation of the dust extinction coefficient from the non-dust extinction coefficient and a solid relationship between the dust extinction coefficient and the fraction

of large particles APC_{280} are of key importance of the INC retrieval. The relationship between dust extinction and APC was intensively studied based on AERONET sun/sky photometer at Morocco, Cape Verde, Barbados, and Cyprus during dust outbreak situations.

5   For the two CALIOP overpass case studies discussed we found good agreement between the ground-based and spaceborne lidar observations. These cases showed in a promising way the potential of lidar to provide tropospheric height profiles of INC. Uncertainties of the order of 25-30 % in the retrieval of the dust extinction coefficient, 20 % in the conversion of the dust extinction coefficients into APC_{280} values, and presently
10 within an order of magnitude in the estimated INC profiles may appear large. However, there is no alternative to provide the atmospheric science community with temporally dense, continuous, coherent, global data sets of INC up to the tropopause than via active remote sensing with ground-based lidar networks in combination with spaceborne lidars.

15 Because there are already several dust-related global studies available based on CALIOP observations (Liu et al., 2008; Tsamalis et al., 2013) with focus on geometrical and optical properties, it should be a comparably easy effort to do the next step towards the characterization of the found aerosol conditions with focus on the potential of the detected dust distributions to trigger heterogeneous ice formation.

20 As an outlook, we need to study to what extend and with what uncertainty the method presented here can also be used for an estimation of INC during situations with dominating fine-mode aerosol, i.e., when a pronounced coarse mode as in the case of desert dust outbreaks is missing. At such conditions, a good and clear correlation of the particle extinction coefficient and APC_{280} might be no longer given.

Dust-related ice nuclei profiling

R. E. Mamouri and A. Ansmann

Title Page

Abstract | Introduction

Conclusions | References

Tables | Figures

⏮ | ⏭

◀ | ▶

Back | Close

Full Screen / Esc

Printer-friendly Version

Interactive Discussion

References

Ansmann, A., Tesche, M., Althausen, D., Müller, D., Freudenthaler, V., Heese, B., Wiegner, M., Pisani, G., Knippertz, P., and Dubovik, O.: Influence of Saharan dust on cloud glaciation in southern Morocco during SAMUM, J. Geophys. Res., 113, D04210, doi:10.1029/2007JD008785, 2008. 25757, 25761

Ansmann, A., Tesche, M., Seifert, P., Althausen, D., Engelmann, R., Fruntke, J., Wandinger, U., Mattis, I., and Müller, D.: Evolution of the ice phase in tropical altocumulus: SAMUM lidar observations over Cape Verde, J. Geophys. Res., 114, D17208, doi:10.1029/2008JD011659, 2009. 25749

de Boer, G., Morrison, H., Shupe, M. D., and Hildner, R.: Evidence of liquid dependent ice nucleation in high-latitude stratiform clouds from surface remote sensors, Geophys. Res. Lett., 38, L01803, doi:10.1029/2010GL046016, 2011. 25749

Bühl, J., Ansmann, A., Seifert, P., Baars, H., and Engelmann, R., Toward a quantitative characterization of heterogeneous ice formation with lidar/radar: comparison of CALIPSO/CloudSat with ground-based observations, Geophys. Res. Lett., 40, 4404-4408, doi:10.1002/grl.50792, 2013. 25749

Cziczo, D. J., Froyd, K. D., Hoose, C., Jensen, E. J., Diao, M., Zondlo, M. A., Smith, J. B., Twohy, C. H., and Murphy, D. M.: Clarifying the dominant sources and mechanisms of cirrus cloud formation, Science, 340, 1320-1324, doi:10.1126/science.1234145, 2013. 25749

DeMott, P. J., Sassen, K, Poellet, M. R., Baumgardner, D., Rogers, D. C., Brooks, S. D., Prenni, A. J., and Kreidenweis, S. M.: African dust aerosols as atmospheric ice nuclei, Geophys. Res. Lett., 30, 1732, doi:10.1029/2003GL017410, 2003. 25757

DeMott, P. J., Prenni, A. J., Richardson, M. S., Kreidenweis, S. M., Twohy, C. H., and Rogers, D. C.: Ice nuclei variability, relation to ambient aerosol properties, and impacts on mixed-phase clouds, in Sixteenth ARM Science Team Meeting Proc., Albuquerque, NM, 27-31 March 2006. 25757

DeMott, P. J., Prenni, A. J., Liu, X., Kreidenweis, S. M., Petters, M. D., Twohy, C. H., Richardson, M. S., Eidhammer, T., and Rogers, D. C.: Predicting global atmospheric ice nuclei distributions and their impacts on climate, P. Natl. Acad. Sci. USA, 107, 11217-11222, doi:10.1073/pnas.0910818107, 2010. 25751, 25755, 25756, 25769

DeMott, P. J., Prenni, A. J., McMeeking, G. R., Sullivan, R. C., Petters, M. D., Tobo, Y., Niemand, M., Möhler, O., Snider, J. R., Wang, Z., and Kreidenweis, S. M.: Integrating laboratory and field data to quantify the immersion freezing ice nucleation activity of mineral dust particles, Atmos. Chem. Phys. Discuss., 14, 17359-17400, doi:10.5194/acpd-14-17359-2014, 2014. 25749, 25756

Holben, B. N., Eck, T. F., Slutsker, I., Tanré, D., Buis, J. P., Setzer, A., Vermote, E., Reagan, J. A., Kaufman, Y. J., Nakajima, T., Lavenu, F., Jankowiak, I., and Smirnov, A.: AERONET - a federated instrument network and data archive for aerosol characterization, Remote Sens. Environ., 66, 1-16, 1998. 25750

Illingworth A.J., Hogan, R. J., O'Connor, E. J., Bouniol, D., Delanoe, J, Pelon, J., Protat, A., Brooks, M. E., Gaussiat, N., Wilson, D. R., Donovan, D. P., Klein Baltink, H., van Zadelhoff, G.-J., Eastment, J. D., Goddard, J. W. F., Wrench, C. L., Haeffelin, M., Krasnov, O. A., Russchenberg, H. W. J., Piriou, J.-M., Vinit, F., Seifert, A., Tompkins, A. M., and Willen, J., CLOUDNET: continuos evaluation of cloud profiles in seven operational models using ground-based observations, B. Am. Meteorol. Soc., 88, 883-898, 2007. 25749

Kamphus, M., Ettner-Mahl, M., Klimach, T., Drewnick, F., Keller, L., Cziczo, D. J., Mertes, S., Borrmann, S., and Curtius, J.: Chemical composition of ambient aerosol, ice residues and cloud droplet residues in mixed-phase clouds: single particle analysis during the Cloud and Aerosol Characterization Experiment (CLACE 6), Atmos. Chem. Phys., 10, 8077-8095, doi:10.5194/acp-10-8077-2010, 2010. 25749

Title Page

Abstract | Introduction

Conclusions | References

Tables | Figures

|◄ | ►|

◄ | ►

Back | Close

Full Screen / Esc

Printer-friendly Version

Interactive Discussion

Kanitz, T., Seifert, P., Ansmann, A., Engelmann, R., Althausen, Casiccia, C., and Rohwer, E. G.: Contrasting the impact of aerosols at northern and southern midlatitudes on heterogeneous ice formation, Geophys. Res. Lett., 38, L17802, doi:10.1029/2011GL048532, 2011. 25749

Liu, D., Wang, Z., Liu, Z., Winker, D., and Trepte, C.: A height resolved global view of dust aerosols from the first year CALIPSO lidar measurements, J. Geophys. Res., 113, D16214, doi:10.1029/2007JD009776, 2008. 25763

Mamouri, R. E., Ansmann, A., Nisantzi, A., Kokkalis, P., Schwarz, A., and Hadjimitsis, D.: Low Arabian dust extinction-to-backscatter ratio, Geophys. Res. Lett., 40, 4762-4766, doi:10.1002/grl.50898, 2013. 25750, 25751, 25761, 25769, 25779

Mamouri, R. E. and Ansmann, A.: Fine and coarse dust separation with polarization lidar, Atmos. Meas. Tech. Discuss., 7, 5173-5221, doi:10.5194/amtd-7-5173-2014, 2014. 25751, 25752, 25753, 25754, 25758, 25760, 25769, 25770

Murray, B. J., O'Sullivan, D., Atkinson, J. D., and Webb, M. E.: Ice nucleation by particles immersed in supercooled cloud droplets, Chem. Soc. Rev., 41, 6519-6554, doi:10.1039/c2cs35200a, 2012. 25749

Martucci, G. and O'Dowd, C. D.: Ground-based retrieval of continental and marine warm cloud microphysics, Atmos. Meas. Tech., 4, 2749-2765, doi:10.5194/amt-4-2749-2011, 2011. 25749

Niemand, M., Möhler, O., Vogel, B., Vogel, H., Hoose, C., Connolly, P., Klein, H., Bingemer, H., DeMott, P., Skrotzki, J., and Leisner, T.: Parameterization of immersion freezing on mineral dust particles: an application in a regional scale model, J. Atmos. Sci., 69, 3077-3092, 2012. 25756

Nisantzi, A., Mamouri, R. E., Ansmann, A., and Hadjimitsis, D.: Injection of mineral dust into the free troposphere during fire events observed with polarization lidar at Limassol, Cyprus, Atmos. Chem. Phys. Discuss., 14, 17299-17329, doi:10.5194/acpd-14-17299-2014, 2014. 25749

Phillips, V. T. J., DeMott, P. J., and Andronache, C.: An emirical parameterization of heterogeneous ice nucleation for multiple chemical species of aerosol, J. Atmos. Sci., 65, 2757-2783, 2008.

Richardson, M. S., DeMott, P. J., Kreidenweis, S. M., Cziczo, D. J., Dunlea, E. J., Jimenez, J. L., Thomson, D. S., Ashbaugh, L. L., Borys, R. D., Westphal, D. L., Casuccio, G. S., and Lersch, T. L.: Measurements of heterogeneous ice nuclei in the western United States

in springtime and their relation to aerosol characteristics, J. Geophys. Res., 112, D02209, doi:10.1029/2006JD007500, 2007. 25749

Sakai, T., Nagai, T., Zaizen, Y., and Mano, Y.: Backscattering linear depolarization ratio measurements of mineral, sea-salt, and ammonium sulfate particles simulated in a laboratory chamber, Appl. Optics, 49, 4441-4449, 2010.

Schmidt, J., Ansmann, A. Bühl, J. Baars, H., Wandinger, U., Müller, D., and Malinka, A. V.: Dual-FOV Raman and Doppler lidar stduies of aerosol-cloud interactions: simultaneous profiling of aerosols, warm-cloud properties, and vertical wind, J. Geophys. Res., 119, L22222, 5512-5527, doi:10.1002/2013JD020424, 2014. 25749

Seifert, P., Ansmann, A., Mattis, I., Wandinger, U., Tesche, M., Engelmann, R., Müller, D., Pérez, C., and Haustein, K.: Saharan dust and heterogeneous ice formation: eleven years of cloud observations at a central European EARLINET site, J. Geophys. Res., 115, D20201, doi:10.1029/2009JD013222, 2010. 25749

Seifert, P., Ansmann, A., Groß, S., Freudenthaler, V., Heinold, B., Hiebsch A., Mattis, I., Schmidt, J., Schnell, F., Tesche, M., Wandinger, U., and Wiegner, M.: Ice formation in ash-influenced clouds after the eruption of the Eyjafjallajökull volcano in April 2010, J. Geophys. Res., 116, D00U04, doi:10.1029/2011JD015702, 2011. 25757

Shupe, M. D.: A ground-based multisensor cloud phase classifier, Geophys. Res. Lett., 34, L22809, doi:10.1029/2007GL031008, 2007. 25749

Tesche, M., Ansmann, A., Müller, D., Althausen, D., Engelmann, R., Freudenthaler, V., and Groß, S.: Vertically resolved separation of dust and smoke over Cape Verde using multiwavelength Raman and polarization lidars during Saharan Mineral Dust Experiment 2008, J. Geophys. Res., 114, D13202, doi:10.1029/2009JD011862, 2009a. 25752, 25753

Tesche, M., Ansmann, A., Müller, D., Althausen, D., Mattis, I., Heese, B., Freudenthaler, V., Wiegner, M., Eseelborn, M., Pisani, G., and Knippertz, P.: Vertical profiling of Saharan dust with Raman lidars and airborne HSRL in southern Morocco during SAMUM, Tellus B, 61, 144-164, doi:10.1111/j.1600-0889.2008.00390.x, 2009b. 25754

Tesche, M., Müller, D., Groß, S., Ansmann, A., Althausen, D., Freudenthaler, V., Weinzierl, B., Veira, A., and Petzold, A.: Optical and microphysical properties of smoke over Cape Verde inferred from multiwavelength lidar measurements, Tellus B, 63, 677-694, doi:10.1111/j.1600-0889.2011.00549.x, 2011. 25754

Tesche, M., Wandinger, U., Ansmann, A., Althausen, D., Müller, D., and Omar, A. H.: Ground-based validation of CALIPSO observations of dust and smoke in the Cape Verde region,

Dust-related ice nuclei profiling

R. E. Mamouri and A. Ansmann

Title Page

Abstract	Introduction
Conclusions	References
Tables	Figures

Back | Close

Full Screen / Esc

Printer-friendly Version

Interactive Discussion

J. Geophys. Res.-Atmos., 118, 2889-2902, doi:10.1002/jgrd.50248, 2013. 25750, 25760, 25780

Tobo, Y., Prenni, A. J., DeMott, P. J., Huffman, J. A., McCluskey, C. S., Tian, G., Pöhlker, C., Pöschl, U., and Kreidenweis, S. M.: Biological aerosol particles as a key determinant of ice nuclei populations in a forest ecosystem, J. Geophys. Res., 118, 10100-10110, doi:10.1002/jgrd.50801, 2013. 25756

Toledano, C., Wiegner, M., Garhammer, M., Seefeldner, M., Gasteiger, J., Müller, D., and Koepke, P.: Spectral aerosol optical depth characterization of desert dust during SAMUM 2006, Tellus B, 61, 216-228, doi:10.1111/j.1600-0889.2008.00382.x, 2009. 25754

Toledano, C., Wiegner, M., Groß, S., Freudenthaler, V., Gasteiger, J., Müller, D., Müller, T., Schladitz, A., Weinzierl, B., Torres, B., and O'Neill, N. T.: Optical properties of aerosol mixtures derived from sun-sky radiometry during SAMUM-2, Tellus B, 63, 635-648, doi:10.1111/j.1600-0889.2011.00573.x, 2011. 25754

Tsamalis, C., Chédin, A., Pelon, J., and Capelle, V.: The seasonal vertical distribution of the Saharan Air Layer and its modulation by the wind, Atmos. Chem. Phys., 13, 11235-11257, doi:10.5194/acp-13-11235-2013, 2013. 25763

Zhang, D., Wang, Z., and Liu, D.: A global view of midlevel liquid-layer topped stratiform cloud distribution and phase partition from CALIPSO and CloudSat measurements, J. Geophys. Res., 115, D00H13, doi:10.1029/2009JD012143, 2011. 25749

Wandinger, U., Seifert, P., Wagner, J., Engelmann, R., Bühl, J., Schmidt, J., Heese, B., Baars, H., Hiebsch, A., Kanitz, T., Althausen, D., and Ansmann, A.: Integrated remote-sensing techniques to study aerosols, clouds, and their interaction Proceedings, 26th International Laser Radar Conference, Volume I, 395-398, Porto Heli, Greece, 25-29 June 2012, 2012. 25749

Winker, D. M., Vaughan, M. A., Omar, A., Hu, Y., Powell, K. A., Liu, Z., Hunt, W. H., and Young, S. A.: Overview of the CALIPSO mission and CALIOP data processing algorithms, J. Atmos. Ocean. Tech., 26, 2310-2323, 2009. 25749, 25750

Dust-related ice nuclei profiling

R. E. Mamouri and A. Ansmann

Table 1. The six steps required to obtain the profile of the ice nuclei concentration from the profile of the particle backscatter coefficient measured with polarization lidar. Indices p, df, dc, and d denote particles, dust fine mode, dust coarse mode, and total dust, respectively. The methods used in the different steps are described in the respective references.

Step	Computed parameter		Reference
1	Particle backscatter coefficient	β_p	Mamouri et al. (2013)
2	Dust fine and coarse-mode backscatter coefficients	β_{df}, β_{dc}	Mamouri and Ansmann (2014)
3	Dust extinction coefficient	$\sigma_{df} + \sigma_{dc}$	Mamouri and Ansmann (2014)
4	Dust APC-extinction relationship		Figs. 1-3
5	Dust APC	$n_{d,280}$	Eq. (1)
6	Dust INC	n_{IN}	Eq. (2), DeMott et al. (2010)

Title Page

Abstract | Introduction

Conclusions | References

Tables | Figures

Back | Close

Full Screen / Esc

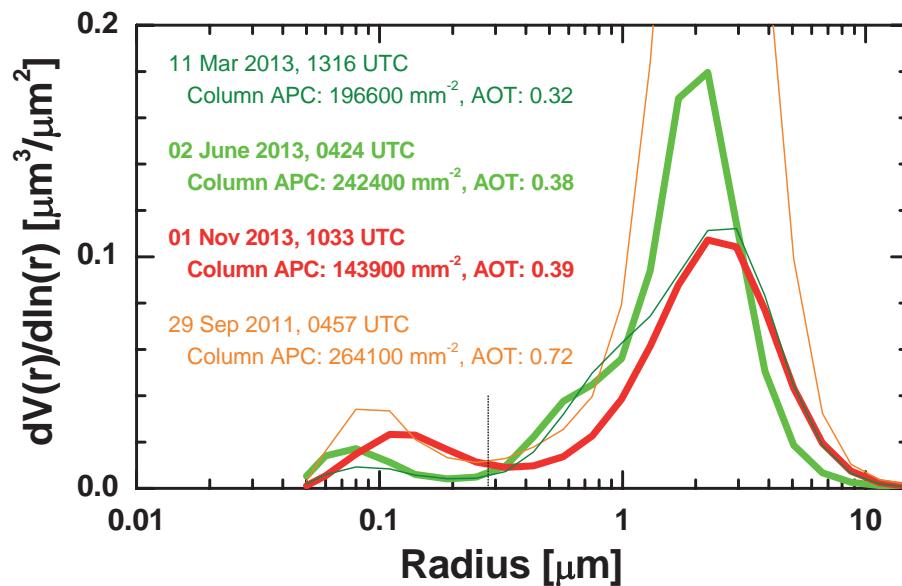Printer-friendly Version

Interactive Discussion
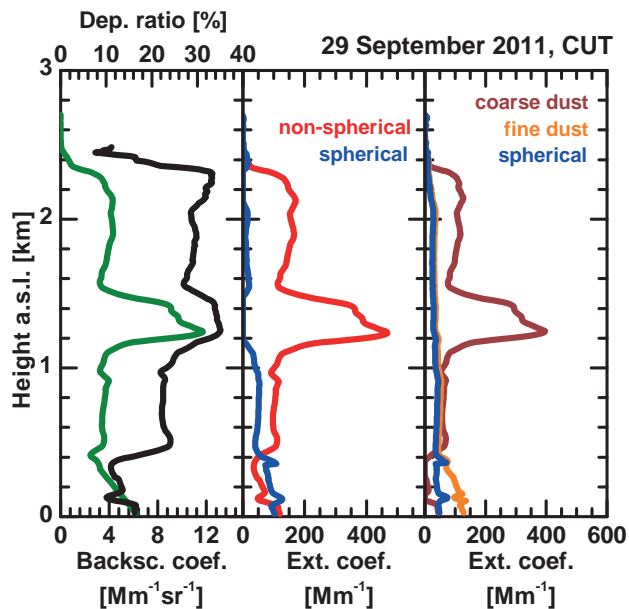
Figure 1. (Left) 532 nm particle backscatter coefficient (green) and particle linear depolarization ratio (black) as a function of height above sea level (a.s.l.), (center) derived particle extinction coefficients separately for non-dust (spherical, blue) and dust (non-spherical, red) by means of the one-step method, and (right) particle extinction coefficients separately for spherical fine-mode (blue), dust fine-mode (orange), and dust coarse-mode particles (deep red) by means of the two-step method. Lidar ratios used in the backscatter-to-extinction conversion are 30 (below 400 m, polluted marine boundary layer) and 60 sr (free troposphere) for the non-dust aerosol component and 40 sr for fine and coarse desert dust. The observation was taken with CUT lidar at Limassol, Cyprus, during a desert dust outbreak from the Middle East on 29 September 2011. Mean profiles for the time period from 07:49-08:29 UTC are shown. The dust outbreak is discussed in detail by Mamouri and Ansmann (2014).

Title Page

Abstract | Introduction

Conclusions | References

Tables | Figures

|◀ | ▶|

◀ | ▶

Back | Close

Full Screen / Esc

Printer-friendly Version

Interactive Discussion

11 Mar 2013, 1316 UTC
Column APC: 196600 mm^{-2}, AOT: 0.32

02 June 2013, 0424 UTC
Column APC: 242400 mm^{-2}, AOT: 0.38

01 Nov 2013, 1033 UTC
Column APC: 143900 mm^{-2}, AOT: 0.39

29 Sep 2011, 0457 UTC
Column APC: 264100 mm^{-2}, AOT: 0.72

Figure 2. Column-integrated particle volume size distribution derived from AERONET sun/sky photometer observations at Limassol. Two Saharan dust cases (11 March 2013, thin olive, 2 June 2013, thick green) and two Middle East desert dust cases (29 September 2011, thin orange, 1 November 2013, thick red) are shown. The short vertical line at 0.28 µm indicates the lower limit of the particle radius range considered in the calculation of column APC_{280}. These column APC_{280} values are given as numbers together with 500 nm total AOT for each case.
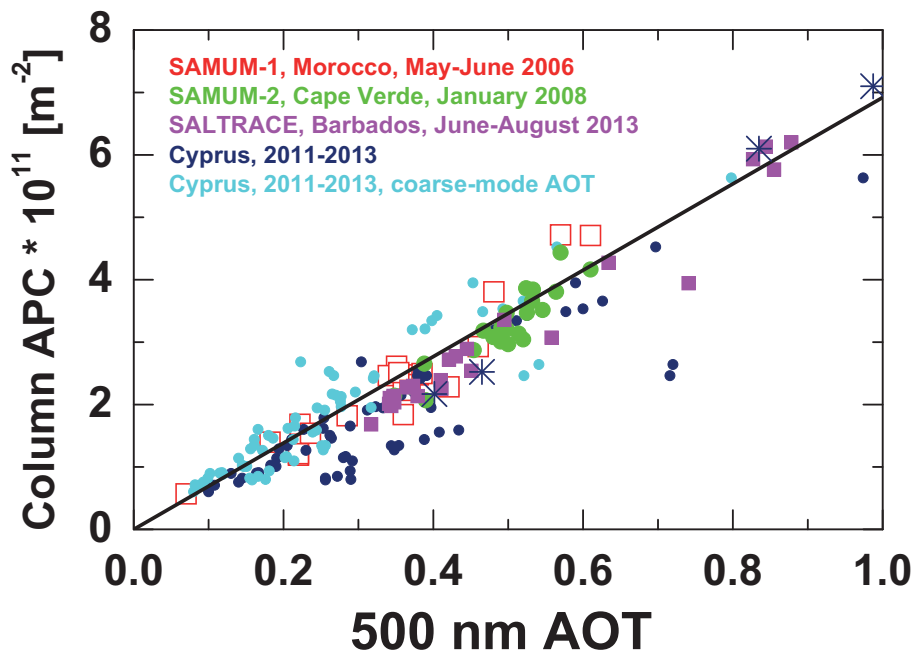
Figure 3. Correlation between aerosol particle optical thickness (500 nm AOT) and column-integrated aerosol particle number concentration (column APC) considering particles with radius > 280 nm only. Desert-dust-dominated observations from several field campaigns (SAMUM-1, large red open squares, SAMUM-2, green circles, SALTRACE, small pink squares) and from long-term observations at Limassol from 2011-2013 are considered. For Cyprus, coarse-mode (light blue circles) and total (fine + coarse-mode, deep blue circles) AOTs are correlated with column APC_{280}. In the case of the stars (4 Cyprus observations with total AOT from 1.6–4), AOT and column APC values are divided by 4.

Discussion Paper | Discussion Paper | Discussion Paper | Discussion Paper |

ACPD

14, 25747–25786, 2014

Dust-related ice nuclei profiling

R. E. Mamouri and
A. Ansmann

Title Page

Abstract | Introduction

Conclusions | References

Tables | Figures

|◄ | ►|

◄ | ►

Back | Close

Full Screen / Esc

Printer-friendly Version

Interactive Discussion
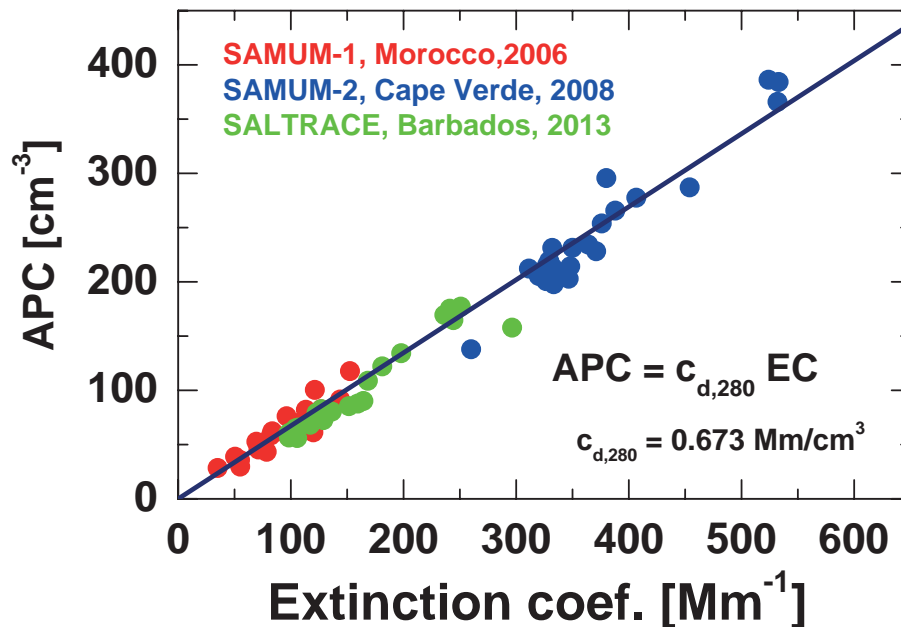
Figure 4. Relationship between dust layer mean 500 nm extinction coefficient (EC) and dust layer mean APC_{280} for observations taken during desert dust field campaigns at Morocco, Cape Verde, and Barbados. The linear regression yields $c_{d,280} = 0.673 \pm 0.07$ Mm cm−3. The correlation coefficient is 0.915. $c_{d,280}$ is used in Eq. (1).
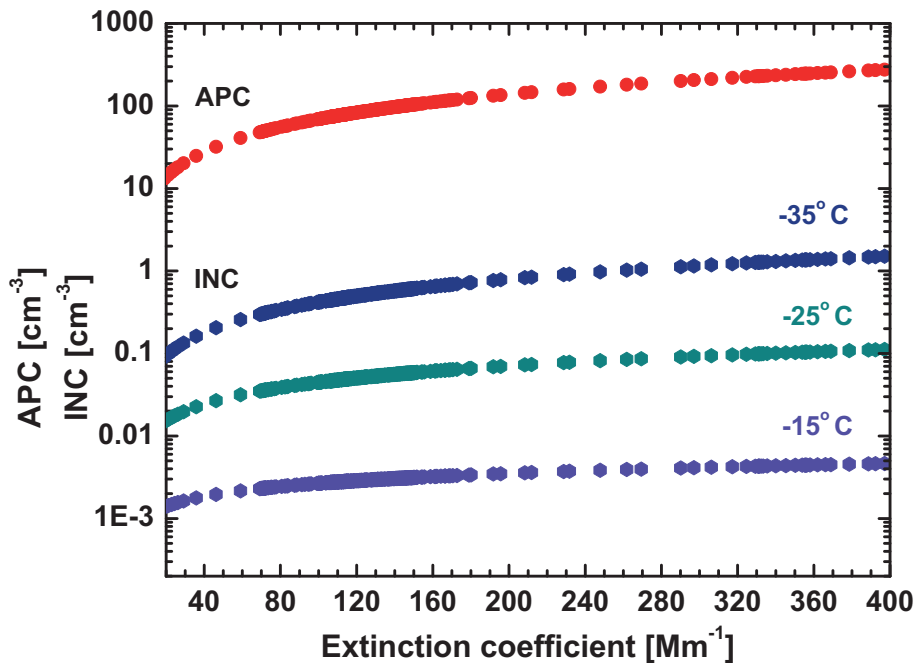
Figure 5. Relationship between total dust extinction coefficient and APC_{280} (red circles) after Eq. (1) and INC after Eq. (2) for temperatures of −15, −25, and −35 °C. The full range of dust extinction coefficients from 30–400 Mm^{-1} measured on 29 September 2011 (Fig. 1) is shown.
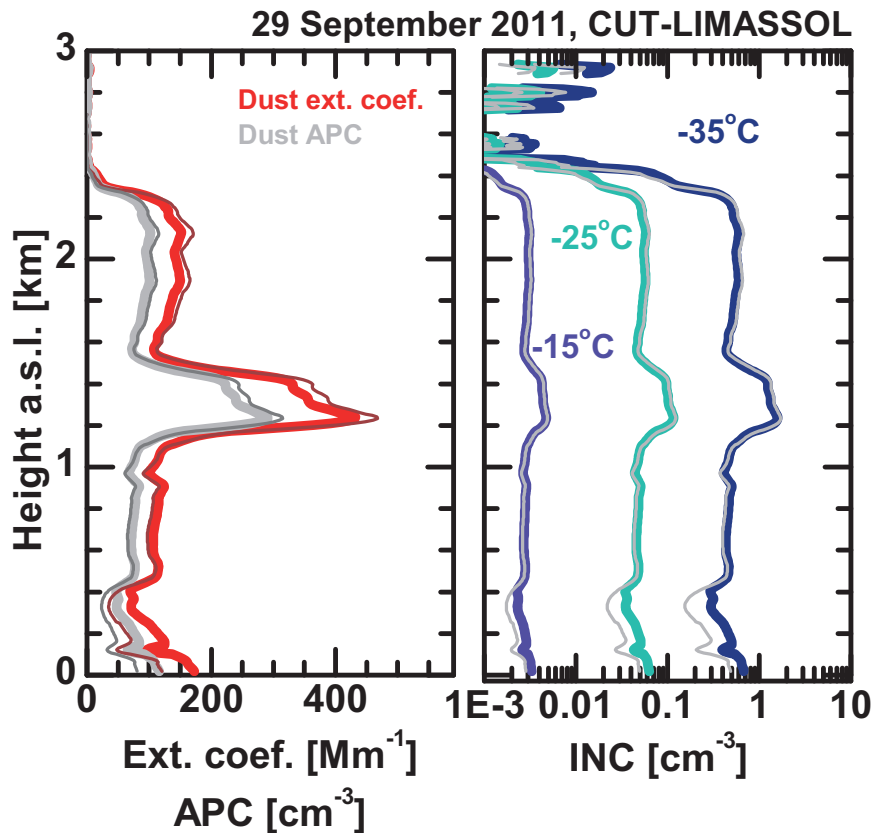
Figure 6. Profiles of 532 nm total dust extinction coefficient (red), APC_{280} (grey), and INC for height-independent temperatures of -15, -25, and $-35\,°C$, derived from the ground-based lidar measurements at Limassol on 29 September 2011 (Fig. 1). In the case of the thick lines, the results are based on the two-step retrieval of the dust extinction coefficient. Respective results obtained by means of the one-step method are shown as thin lines.
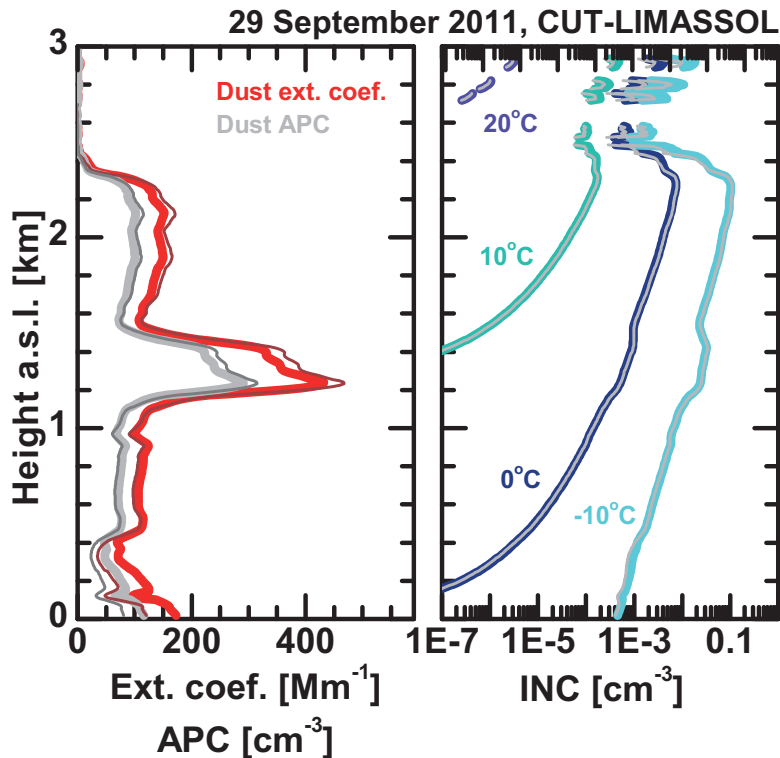
Figure 7. Profiles of 532 nm total dust extinction coefficient (red), APC_{280} (grey), and INC by assuming Standard Atmosphere temperature profiles (temperature gradient of $-0.008\,\mathrm{K\,m^{-1}}$) with surface temperatures of -10, 0, 10, and $20\,^{\circ}\mathrm{C}$ at $0\,\mathrm{m}$ height a.s.l. Dust extinction profiles were measured at Limassol on 29 September 2011. In the case of the thin and thick lines, the results are based on the one-step and the two-step retrieval of the dust extinction coefficient, respectively. Uncertainties in the retrieval products are 25–30 % (extinction coefficient), 30–40 % (APC_{280}), and within a factor of 10 (INC).

Title Page

Abstract | Introduction

Conclusions | References

Tables | Figures

◄ | ►|

◄ | ►

Back | Close

Full Screen / Esc

Printer-friendly Version

Interactive Discussion
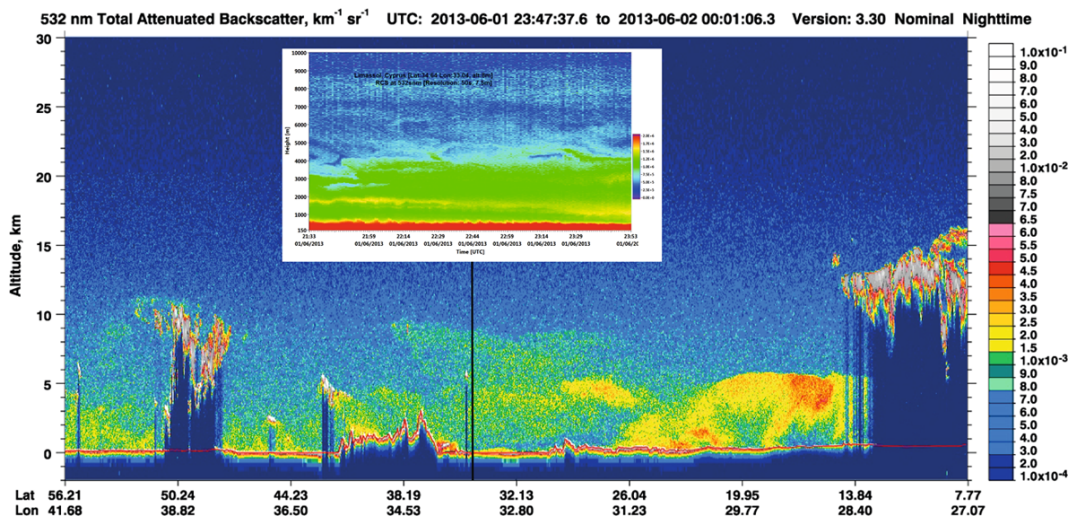
Figure 8. CALIOP measurement (height versus latitude/longitude display) of the attenuated 532 nm particle backscatter coefficient during an overpass 45 km to the east of Limassol on 1 June 2013, 23:47 UTC, to 2 June 2013, 00:01 UTC. Desert dust layers are given in green to yellow colors and reach up to 4–10 km height. The inserted height-time display shows the CUT lidar observation of the range-corrected cross-polarized 532 nm backscatter lidar signal on 1 June 2013, 21:33-23:53 UTC (height range from 250-10000 m a.s.l.). Dust (green, yellow, and light blue layers) is observed up to 9-10 km height. The vertical black line indicates the closest position of CALIOP (laser foot print) to the ground-based CUT lidar at Limassol, Cyprus.
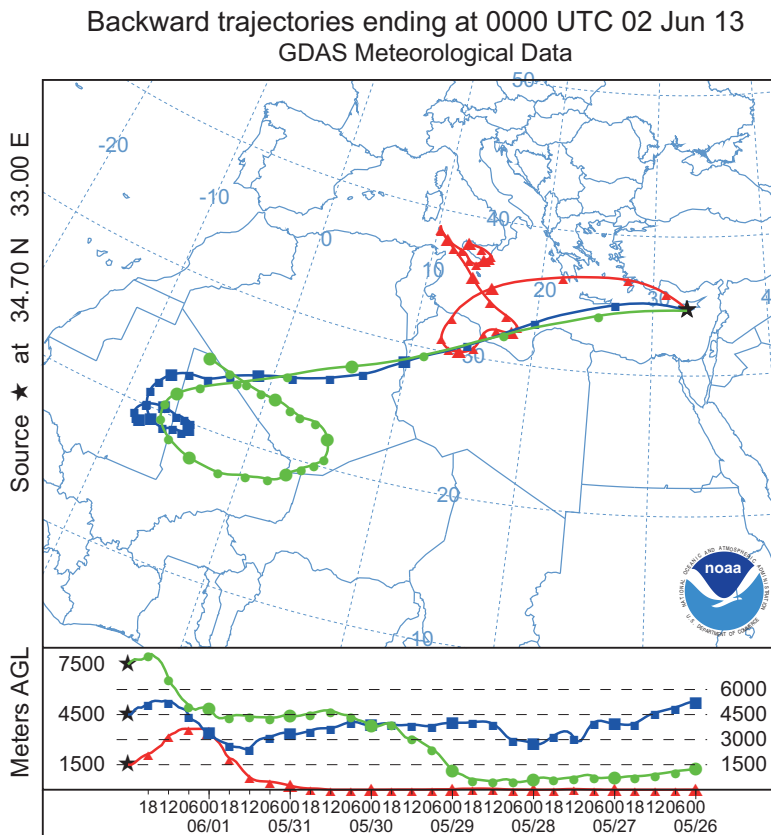
Figure 9. HYSPLIT 7-day backward trajectories arriving within the dust layer over Limassol, Cypurs, at 1500 (red), 4500 (blue), and 7500 m height (green) on 2 June 2013, 00:00 UTC.
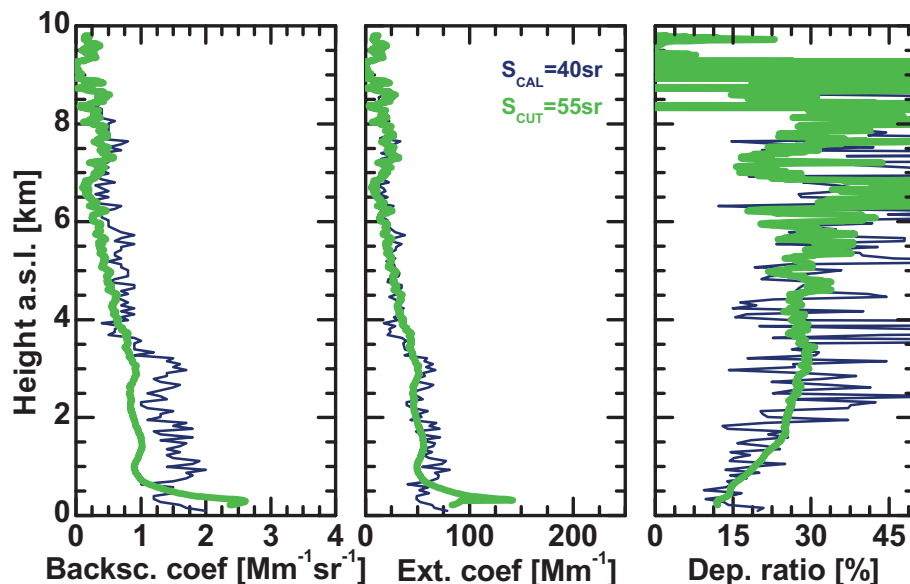
Figure 10. Comparison of profiles of particle backscatter coefficient, extinction coefficient, and particle linear depolarization ratio measured with ground-based CUT lidar at Limassol (thick green curves, 60 min means) on 1 June 22:28–23:28 UTC, and with spaceborne CALIOP (black noisy curves, 45 km east of Limassol, during seconds 38–43 of 23:53 UTC). In the case of CALIOP, 135 signal profiles are averaged (nine level-2 aerosol profiles, 45 km horizontal resolution). No vertical smoothing is applied to the CALIOP data. CUT lidar signal profiles were vertically smoothed by 180 m. A lidar ratio (height-independent over the entire tropospheric range) of S_{CAL} = 40 sr was selected in the retrieval of CALIOP data and of S_{CUT} = 55 sr (optimum lidar ratio for this Saharan dust case from the combined lidar/photometer analysis after Mamouri et al. (2013)) was applied in the CUT computation of backscatter and extinction profiles.
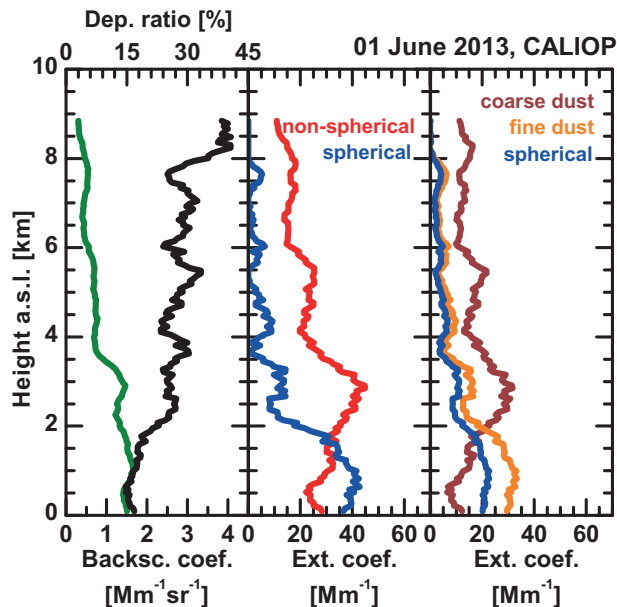
Figure 11. CALIOP data analysis products based on the 135 signal profile averages shown in Fig. 10: (Left) Vertical profiles of 532 nm particle backscatter coefficient (green) and particle linear depolarization ratio (black), (center) derived particle extinction coefficients (one-step method) separately for non-dust (spherical, blue) and dust (non-spherical, red), and (right) particle extinction coefficients (two-step method) separately for spherical fine-mode (blue), dust fine-mode (orange), and dust coarse-mode particles (deep red). The total particle backscatter coefficients (left, green) are taken from the CALIOP data base and smoothed with 600 m gliding window length. The particle linear depolarization ratio is computed from the smoothed CALIOP backscatter profiles after Tesche et al. (2013). The cross-polarized and total backscatter coefficient profiles are smoothed with 600 m vertical window length. Lidar ratios used in the backscatter-to-extinction conversion are 50 sr for the non-dust aerosol component and 55 sr for fine and coarse dust.
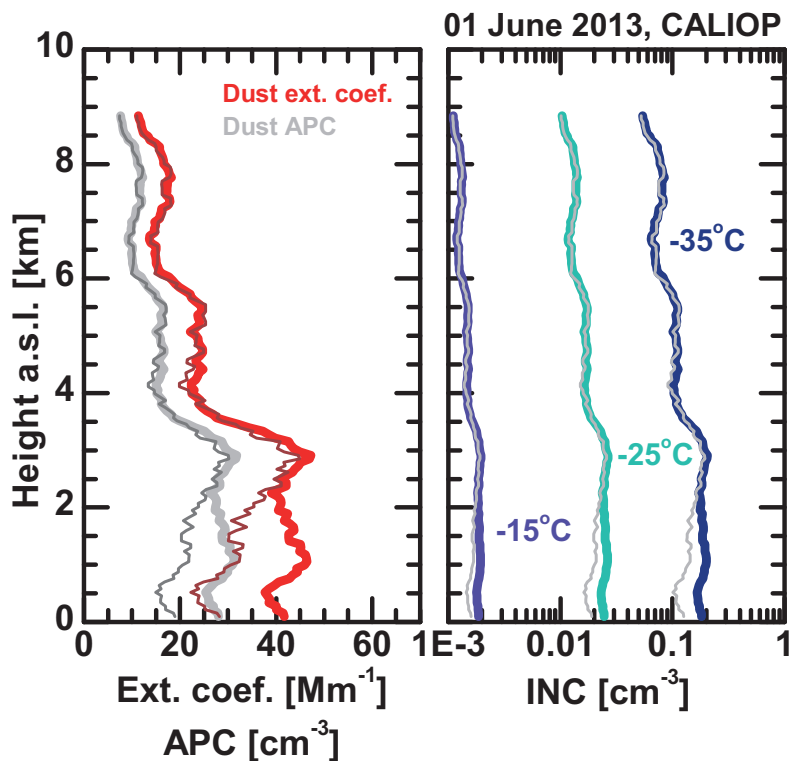
Title Page

Abstract | Introduction

Conclusions | References

Tables | Figures

◄ | ►

◄ | ►

Back | Close

Full Screen / Esc

Printer-friendly Version

Interactive Discussion

Figure 12. Profiles of 532 nm total dust extinction coefficient (red), APC_{280} (grey), and INC for height-independent temperatures of -15, -25, and $-35\,°C$, derived from the CALIOP observations (Fig. 11) on 1 June 2013. In the case of the thick lines, the results are based on the two-step retrieval of the dust extinction coefficient. Respective results obtained by means of the one-step method are shown as thin lines. Uncertainties are 25–30 % (extinction coefficient) and 30–40 % (APC_{280}) for heights > 2 km, and within a factor of 10 in the case of INC.
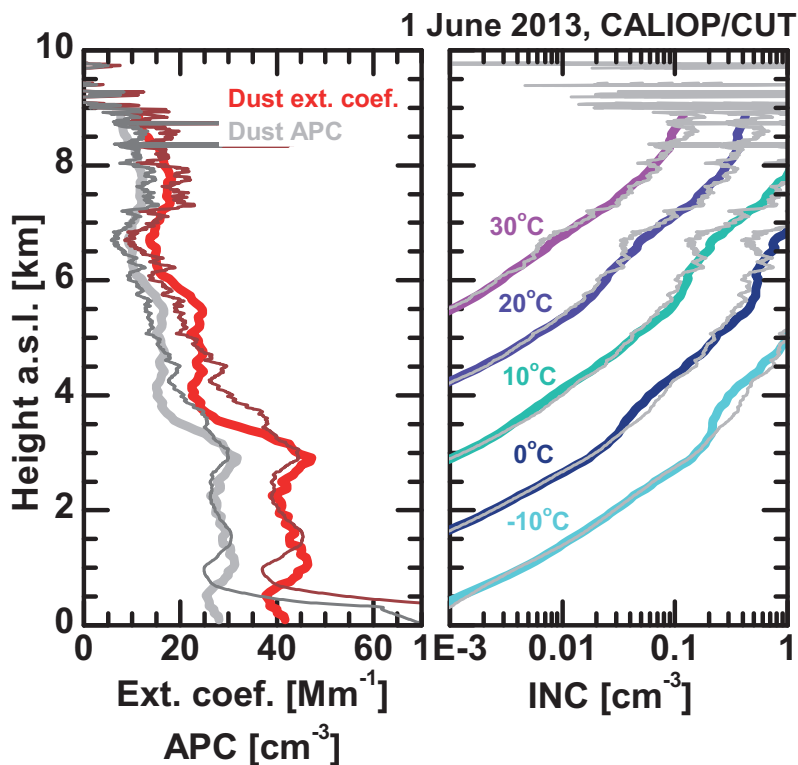
Title Page

Abstract | Introduction

Conclusions | References

Tables | Figures

|◄ | ►|

◄ | ►

Back | Close

Full Screen / Esc

Printer-friendly Version

Interactive Discussion

Figure 13. Profiles of 532 nm total dust extinction coefficient (by means of the two-step method), APC_{280}, and INC by assuming a Standard Atmosphere temperature profile (temperature gradient of $-0.008\,K\,m^{-1}$) with surface temperatures of -10, 0, 10, 20, and $30\,°C$ at $0\,m$ height a.s.l. Ground-based CUT lidar results (thin lines) are compared with respective CALIOP retrieval results (thick lines). The actual $2\,m$ air temperature was between 20-30 °C. Uncertainties are 25–30 % (extinction coefficient), 30–40 % (APC_{280}), and within a factor of 10 (INC).
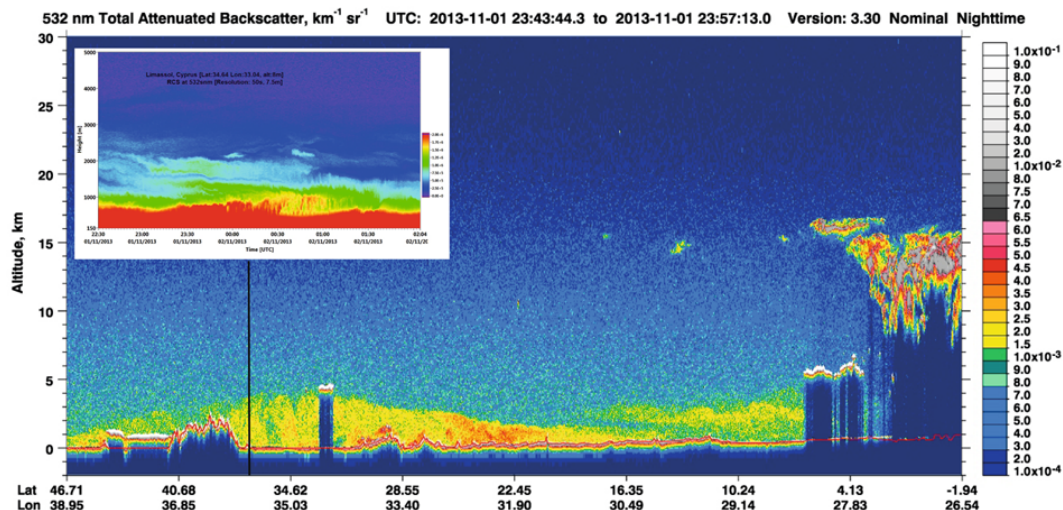
Figure 14. CALIOP measurement (height versus latitude/longitude display) of the attenuated 532 nm particle backscatter coefficient during an overpass 180 km to the east of Limassol on 1 November 2013, 23:43–23:57 UTC. Desert dust layers are given in green to yellow colors and reach up to about 4 km height. The inserted height-time display shows the CUT lidar observation of the cross-polarized range-corrected 532 nm backscatter signal up to 5 km height on 1 November 2013, 22:30 to 2 November 2013, 02:04 UTC. The vertical black line indicates the closest position of CALIOP (laser foot print) to the ground-based CUT lidar at Limassol, Cyprus.
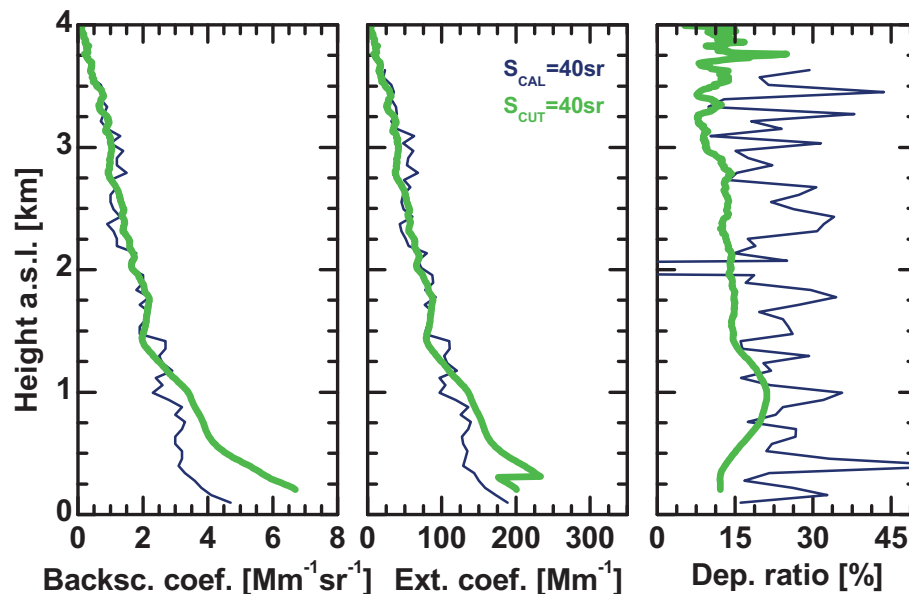
Figure 15. Comparison of profiles of particle backscatter coefficient, extinction coefficient, and particle linear depolarization ratio measured with ground-based CUT lidar at Limassol (thick green curves, 60 min means) on 2 November 2013, 00:00–00:59 UTC and with spaceborne CALIOP (black noisy curves, 180 km east of Limassol, during seconds 8–14 of 23:47 UTC of 1 November 2013). In the case of CALIOP, 135 signal profiles are averaged (nine level-2 aerosol profiles, 45 km horizontal resolution). No vertical smoothing is applied to the CALIOP data. CUT lidar signal profiles were vertically smoothed by 180 m. A lidar ratio (height-independent over the entire tropospheric range) of $S_{CAL} = 40$ sr was selected in the retrieval of CALIOP data as well as in the computation of CUT lidar backscatter and extinction profiles ($S_{CUT} = 40$ sr) for this Middle East desert dust case.

Title Page

Abstract | Introduction

Conclusions | References

Tables | Figures

|◄ | ►|

◄ | ►

Back | Close

Full Screen / Esc

Printer-friendly Version

Interactive Discussion
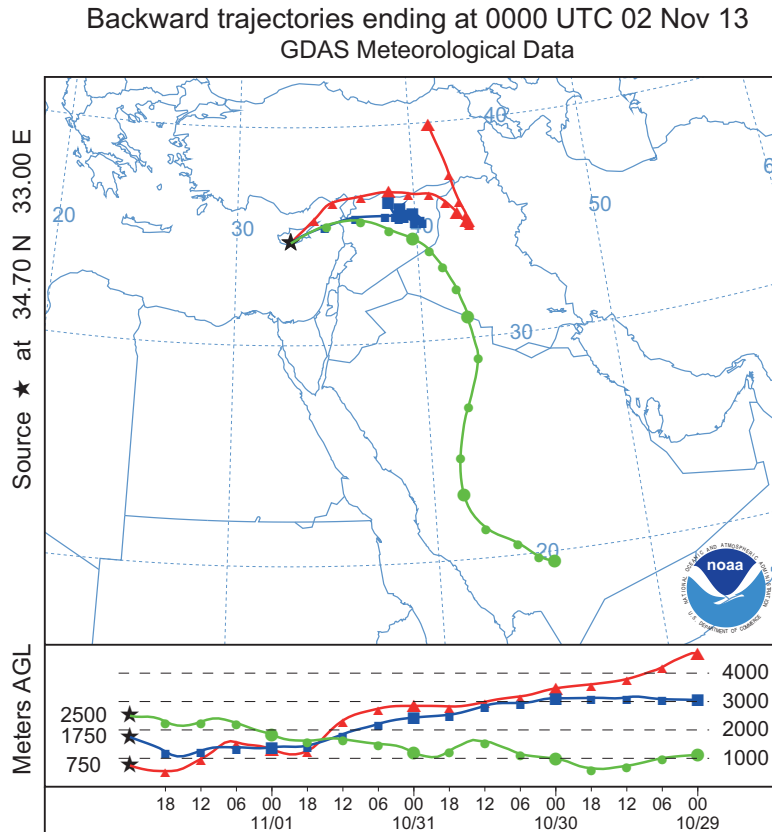
Figure 16. HYSPLIT 4 day backward trajectories arriving within the dust layer over Limassol, Cyprus, at 750 (red), 1750 (blue), and 2500 m height (green) on 2 November 2013, 00:00 UTC.
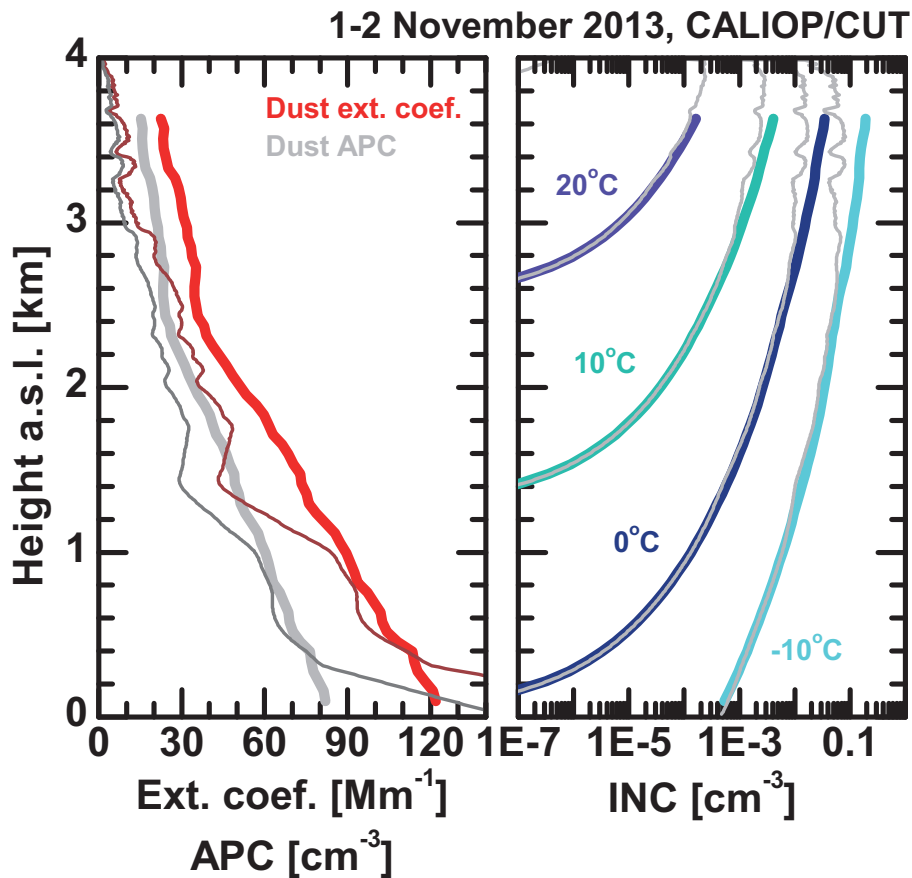
Figure 17. Same as Fig. 13, except for the observations on 1–2 November 2013. Ground-based CUT lidar results (thin lines) are compared with respective CALIOP retrieval results (thick lines). Uncertainties are 25–30 % (extinction coefficient), 30–40 % (APC_{280}), and within a factor of 10 (INC).

Title Page

Abstract | Introduction

Conclusions | References

Tables | Figures

|◄ | ►|

◄ | ►

Back | Close

Full Screen / Esc

Printer-friendly Version

Interactive Discussion